Electron correlation in the decay of resonantly excited $3d^{-1}_{3/2,5/2}5p$ states of krypton

H. Aksela, J. Jauhiainen, E. Kukk, E. Nõmmiste, and S. Aksela
Department of Physical Sciences, University of Oulu, FIN-90570 Oulu, Finland
and the Finnish Synchrotron Radiation Facility at MAX-lab, Box 118, S-22100 Lund, Sweden

J. Tulkki
Optoelectronics Laboratory, Helsinki University of Technology, FIN-02150 Espoo, Finland
(Received 14 July 1995)

The deexcitation of the resonantly excited Kr $3d^{-1}_{3/2,5/2}5p$ states has been studied by recording the electron spectra with very high photon and electron energy resolution and by comparing the results with multiconfiguration Dirac-Fock calculations. The high resolution has enabled us to resolve the fine structures in detail by utilizing the Auger resonant Raman effect. High-quality experimental results are used to confirm the roles of exchange interaction and of initial- and final-state interactions in distributing the intensity to the fine structures in the spectra.

PACS number(s): 32.80.Hd, 32.80.Fb

I. INTRODUCTION

Auger resonant Raman spectroscopy, since it was for the first time detected at the VUV region [1], has proven to be a very powerful method to reveal finest details in the intensity distribution of the resonant Auger transitions [2–4]. The Xe $4d^{-1}6p \rightarrow 5p^{-2}6p$ transitions investigated in detail recently in [2,3] and the Kr $3d^{-1}5p \rightarrow 4p^{-2}5p$ transitions studied in this work are extremely sensitive to the influence of the spectator-core coupling, which substantially alters the strength of initial- and final-state correlation effects.

High photon energy resolution, combined with high-brilliance undulator radiation at the Finnish beamline (BL51) at MAX-laboratory [5,6], has allowed us to substantially diminish the linewidth by exciting only a narrow portion of the lifetime-broadened absorption resonance. Full benefit from the use of the Auger resonant Raman effect comes up when the outer subshells are involved in the transitions. In such a case the spectator-core interaction is of real importance as compared to the core-core interaction. Furthermore, when the resolution of the electron spectrometer is high enough, it becomes possible to resolve all the line components created via the spectator-core coupling.

Low kinetic energies of Kr and Xe Auger electrons make them very sensitive to the potential used in the calculation of continuum electrons. The role of the exchange interaction between the core and continuum electrons is of special interest. Initial- and final-ionic-state configuration interactions (IISCI and FISCI) also substantially affect the partial transition rates [7]. Comparison with high-quality experimental results allows us to confirm the roles of various contributions in reproducing the experiment. Moderate resolution would smear out the details that are of crucial importance in testing the theory. Electron correlation effects are of similar origin but slightly changed in passing from Kr to Xe spectra, which makes it possible to find more general trends when comparing the two results with each other. We first discuss the Kr $3d^{-1}5p \rightarrow 4p^{-2}5p$ transitions in detail and then make a comparison with the previous Xe results [2,3].

II. EXPERIMENT

A. Measurements

The measurements were performed at the Finnish beamline at MAX-laboratory in Lund, Sweden. A detailed description of the beamline has been published elsewhere [5,6]. Briefly, the beamline uses synchrotron radiation from an undulator [8,9] in the photon energy range of 60–600 eV, and it has a modified SX-700 plane grating monochromator [10] with a plane elliptical focusing mirror. The beamline contains a permanent differential pumping section designed to isolate effectively the high-pressure gas experiments from the ultrahigh vacuum of the monochromator. This section includes also a toroidal refocusing mirror in order to get a small spot size ($\emptyset \approx 1$ mm) in the source point of the electron spectrometer.

The electron spectrometer SES-144 [11] has a hemispherical electron analyzer provided with a four-element retarding electron lens. The position-sensitive detector uses a microchannel plate detector from which electron pulses are accelerated onto a fluorescent screen, and the resulting optical flashes are scanned using a charge-coupled-device (CCD) TV camera. The pressure in the sample compartment is on the order of 10^{-3}–10^{-4} mbar. The resolution of the electron spectrometer at 10-eV pass energy is about 35 meV; and at 5-eV pass energy, about 25 meV. The resolution is mainly limited by the electrical noise ($\sim$30 meV) of the laboratory.

The used undulator radiation is almost completely linearly polarized. The electron analyzer has been mounted with the principal axis of the electron lens in the magic angle of 54.7° versus the electric field vector of the incoming radiation, which allows angular-independent measurements of branching ratios. An almost complete absence of higher-order contributions in the exciting undulator radiation forms a further important advantage. The broadening contribution from the monochromator is estimated to be 11.3 and 13.4 meV for 10- and 20-μm exit slit sizes, respectively.

B. Experimental results

Figure 1 shows the ejected electron spectra of Kr taken at $h\nu = 91.200$ eV (a) and $h\nu = 92.425$ eV (b) that correspond to

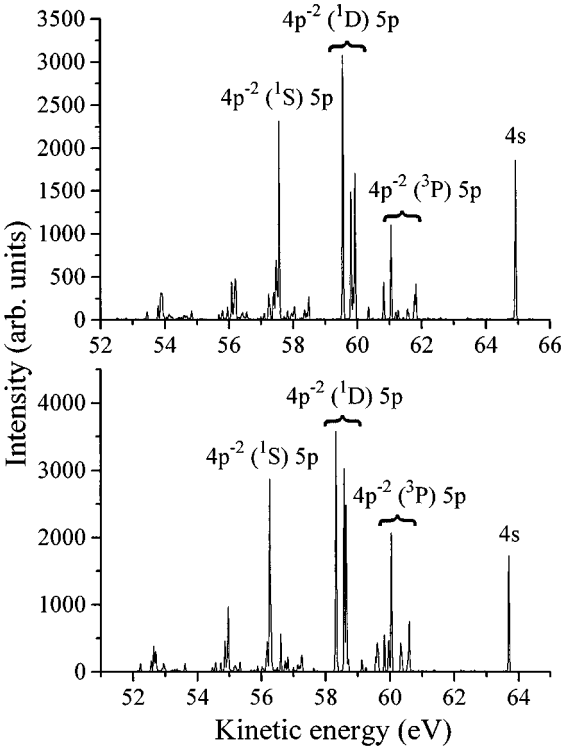

FIG. 1. Lower part: the electron spectrum of Kr excited by 91.200-eV photons corresponding to the $3d_{5/2}\rightarrow 5p$ excitation. Upper part: the electron spectrum of Kr excited by 92.425-eV photons corresponding to the $3d_{3/2}\rightarrow 5p$ excitation. The spectra were measured with a pass energy of 10 eV corresponding to an electron spectrometer resolution of 35 meV.

the maxima of the $3d_{5/2}\rightarrow 5p$ and $3d_{3/2}\rightarrow 5p$ photoexcitation resonances [12], respectively. The spectra of Fig. 1 were measured with a pass energy of 10 eV and a monochromator exit slit size of 20 μm. As compared with the spectra reported in Ref. [13], the overall features are the same but the resolution in the present experiment is much better, which can be seen from the fact that several peaks are further split in the present spectra. A second set of spectra was recorded with a pass energy of 5 eV and a 10-μm slit size. No essential differences were observed between the two recordings. Only the resolution improved when the retardation was increased, reducing the linewidth from 48 to 40 meV. Kinetic energy calibration of the spectra was achieved by determining the energies with the aid of photoexcitation energies from Ref. [12] and the final-state binding energies given in optical data [14].

The spectra have been corrected for the spectrometer transmission by using an experimentally determined correction function [15]. The energies and relative intensities of the lines were determined by using a least-squares fit with Voigt functions. The energy separation of individual lines was taken from the energy splitting of the final-state levels determined by optical measurements [14] and kept fixed during the fitting procedure. The valence photoelectron satellite lines were also included in the fit. The fitting results are presented in Table I, and Figs. 2 and 3 display the detailed decomposition of peaks that contain transitions to the $4p^{-2}(^3P)5p$ and $4p^{-2}(^1D)5p$ final states. Error limits in Table I were determined from the deviation between the fitting results of separately measured spectra. Because of the close proximity of lines 7 to 9 and of lines 16 to 18, their

TABLE I. Experimental energies and intensities of the Kr $3d^{-1}5p\rightarrow 4p^{-5}5p$ resonant Auger electron lines. The intensities are given as percentages of the total intensity. The listed terms are the leading LS terms, which, because of a large mixing of the states, should be considered only as tags of the final states.

Final ionic state		Line	$3d_{5/2}^{-1}5p$		$3d_{3/2}^{-1}5p$	
Parent	Term	in expt.	Energy (eV)	Intensity (%)	Energy (eV)	Intensity (%)
$4p^4(^3P)5p$	$^4P_{5/2}$	1	60.597	4.2±0.5	61.822	2.7±0.3
	$^4P_{3/2}$	2	60.552	0.9±0.2	61.777	1.8±0.2
	$^4D_{7/2}, ^4P_{1/2}$	3	60.367	1.6±0.1	61.592	0.5±0.1
	$^2D_{5/2}$	4	60.331	2.4±0.1	61.556	0.8±0.1
	$^2D_{3/2}$	5	60.045	11.0±0.8	61.270	0.8±0.1
	$^2P_{1/2}$	6	59.955	2.2±0.2	61.180	0.1±0.1
	$^2P_{1/2}$	7	59.824	1.3±0.3	61.049	3.3±0.6
	$^2P_{3/2}$	8	59.827	0.8±0.2 } 2.5±0.3	61.052	2.6±0.4 } 8.1±0.4
	$^4D_{5/2}$	9	59.830	0.4±0.2	61.055	2.3±0.3
	$^4D_{1/2}$	10	59.551	1.1±0.2	60.776	0.1±0.1
	$^4S_{3/2}$	11	59.597	2.2±0.4	60.822	2.8±0.3
	$^4D_{3/2}$	12	59.631	1.7±0.3	60.856	0.2±0.1
$4p^4(^1D)5p$	$^2F_{5/2}$	13	58.706	0.8±0.1	59.931	13.3±1.1
	$^2F_{7/2}$	14	58.641	13.4±1.8	59.866	2.5±0.1
	$^2P_{3/2}$	15	58.579	16.5±2.1	59.804	10.5±0.8
	$^2D_{5/2}$	16	58.317	8.9±1.4	59.542	7.9±1.6
	$^2P_{1/2}$	17	58.326	3.9±1.8 } 20.2±3.5	59.551	7.1±2.1 } 26.1±1.4
	$^2D_{3/2}$	18	58.332	7.4±1.1	59.557	11.1±0.8
$4p^4(^1S)5p$	$^2P_{1/2}$	19	56.339	0.2±0.2	57.564	21.0±2.9
	$^2P_{3/2}$	20	56.256	16.2±1.8	57.481	3.8±0.8

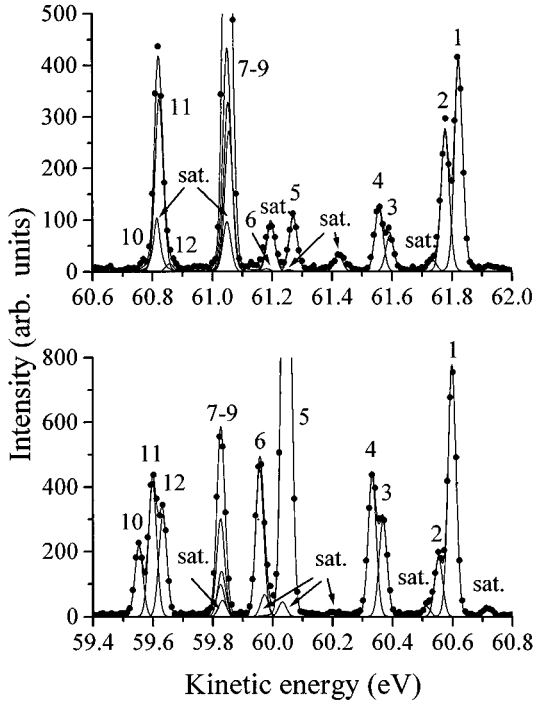

FIG. 2. Kinetic energy region of the $3d^{-1}5p \rightarrow 4p^{-2}(^3P)5p$ spectator Auger electron spectrum of Kr (lines 1–12 in Table I) excited by 91.200-eV (lower part) and 92.425-eV (upper part) photons, corresponding to the $3d_{5/2}^{-1} \rightarrow 5p$ and $3d_{3/2}^{-1} \rightarrow 5p$ excitations, respectively.

individual error limits are extremely large. Only the total intensity of the three lines in both peaks can thus be regarded as a reliable value for comparison with theory.

An interesting feature in the results is that the spectra taken at the two photon energies differ distinctly from each other, especially in the way the intensity is distributed among all the fine-structure levels. The difference is considerably larger in the case of resonant Auger electron spectra than in the case of normal Auger electron spectra, where the $3d_{5/2}$ or $3d_{3/2}$ core-hole states, instead of core-excited states, decay via two-electron transitions.

III. CALCULATIONS

A. Computational method

The calculations of transition energies and partial transition rates for the resonant Auger process in Kr were performed by using a single-channel multiconfiguration Dirac-Fock (MCDF) approach, described in details in Refs. [7,16,17]. Results of similar calculations were recently compared with the experiment in the case of the $4d^{-1}6p \rightarrow 5p^{-2}6p$ transitions of Xe [2,3]. Here we present only a short summary of the actual calculations; for further details the reader is referred to Ref. [7].

We assume a two-step description for the Auger effect and neglect the direct transition amplitudes to the final states of the Auger decay. This can be considered a reasonably good approximation in the present case since the population of odd parity configurations $4p^{-2}np$ via direct photoionization channels is small.

In all calculations, the initial and final states of the decay were described by multiconfiguration wave functions accounting for IISCI and FISCI. For the initial state we included three jj-coupled configurations $3d_{5/2}^{-1}5p_{3/2}, J=1$, $3d_{3/2}^{-1}5p_{1/2}, J=1$, and $3d_{3/2}^{-1}5p_{3/2}, J=1$. For the final state all the jj-coupled configurations that result from the nonrelativistic configurations $4s^{-2}5p$, $4s^{-1}4p^{-1}5p$, $4p^{-2}5p, 4s^{-1}$, and $4p^{-1}$ were included. The spectator orbital was obtained in the same self-consistent-field (SCF) calculation as the core orbitals. The continuum orbital was calculated in a jj-average field of the core plus spectator electron and made orthogonal to the bound orbitals by Lagrangian multipliers, except in one calculation (referred to as F) that excludes the exchange interaction.

To study the importance of exchange interaction and the influence of the orbital set to the partial transition rates, the calculations were carried out in different approximations as follows. First, the effect of exchange interaction between the continuum and bound electrons was studied by using the bound orbitals optimized for the final ionic state but neglecting (F) or including (FE) the exchange potential in the calculation of the continuum orbitals. Also the mixing coefficients appearing in the initial-state multiconfiguration wave function were calculated by using final-state orbitals in the diagonalization of the initial-state Hamiltonian. The influence of the choice of one-electron orbitals was studied by comparing the FE values with results obtained by using the bound orbitals optimized for the initial excited state in the final-state wave function, as well as in determination of the final ionic state mixing coefficients (approximation IE).

Whereas the approximations FE and IE are based on the use of an orthogonal set of one-electron orbitals, our approximation FEI does not conserve the orthogonality of many-electron wave functions exactly. In FEI, different basis sets were used in the calculation of initial- and final-state mixing coefficients even though the orbitals optimized for the final state were otherwise used. The contribution of orbital relaxation through the mixing coefficients is thus included in FEI, even though the nonorthogonality is not fully accounted for. To study the importance of IISCI, the calculations were additionally carried out by completely omitting the mixing of initial jj-coupled configurations in approximation FEO.

B. Results of calculations

The energies of the transitions were obtained as the difference between the initial- and final-state SCF energies (the $\triangle E_{\mathrm{SCF}}$ approach). The results for the $3d_{5/2}^{-1}5p_{3/2}, J=1 \rightarrow 4p^{-2}5p$ transitions are given in Table II. The energetic order of the levels and the magnitude of the splitting was found to be very sensitive to the basis set used in calculations. The jj-coupled SCF's were found to be strongly mixed both in the initial and final state of the decay, but the coupling scheme was still far from the LS-coupling limit. Therefore the LS symbols, given in the tables, should be considered only as tentative tags for the final states, where the total angular momentum J is the only reliable quantum number. The LS symbols given in the literature may differ from each other, which only indicates the sensitivity of the

FISCI to the orbital set used in calculations but does not mean any reassignment of states.

The population of initial states, achieved via photoexcitation, is restricted to three atomic states with $J=1$ (referred to as A, B, and C hereafter), according to the dipole selection rules. The first well separated state A is mainly due to the $3d_{5/2}^{-1}5p_{3/2},J=1$ configuration, whereas the closely spaced states B and C involve a strong mixing of $3d_{3/2}^{-1}5p_{1/2},J=1$ and $3d_{3/2}^{-1}5p_{3/2},J=1$ configurations. The SCF calculations for the initial state yielded a separation of 1.272 eV between the A and B and 0.031 eV between states B and C. According to the photoexcitation probabilities predicted by the GRASP code [18], the population of state B is, however, 20 times larger than the population of state C. States A and B can thus be regarded as the initial states for the subsequent resonance Auger transitions, whereas the decay via state C plays only a minor role.

In Table II we list the partial transition rates for the initial state A calculated in approximations F, FE, and IE. Since these transitions are free from IISCI, they are well suited to study the sensitivity of the intensities to the exchange, relaxation, and FISCI. For comparison, the values of calculations similiar to our approach F, reported by Chen [19], are also depicted. The exchange effect seems to result in a general decrease of the absolute transition rates, whereas the changes in relative transition rates are much larger between the FE and IE results. The FISCI thus plays a prominent role in branching ratios, whereas the total rates are more strongly affected by the exchange interaction.

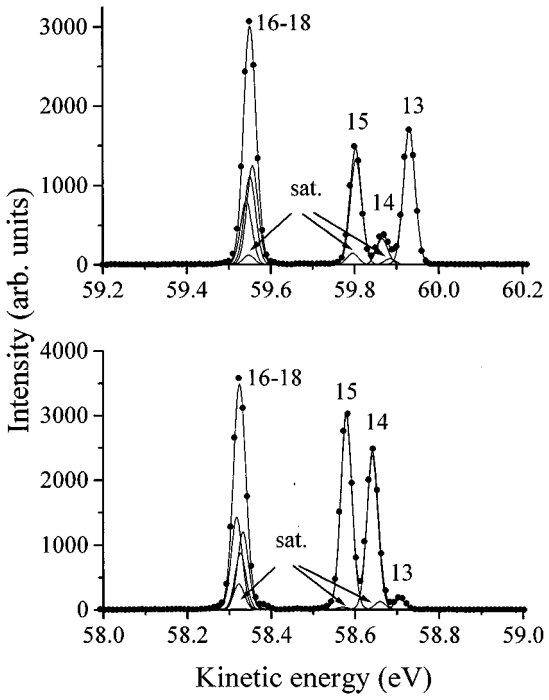

FIG. 3. Kinetic energy region of the $3d^{-1}5p\rightarrow 4p^{-2}(^1D)5p$ resonant Auger electron spectrum of Kr (lines 13–17 in Table I). For details see the caption of Fig. 2.

TABLE II. Calculated energies and intensities for the Kr $3d_{5/2}^{-1}5p\rightarrow 4p^{-2}5p$ resonant Auger transitions. F indicates single-channel results obtained using final-state orbitals and excluding the exchange for the continuum electron. The FISCI was computed by using final state orbitals. FE is the same as F but the exchange was included. IE indicates single-channel values obtained using initial-state orbitals with exchange. The FISCI was calculated by using initial-state orbitals.

Final ionic state		Line	Energy (eV)		Intensity (10^{-3} a.u.)			
Parent	Term	in expt.	Calc.	Expt.	F	FE	IE	Chen [19]
$4p^4(^3P)5p$	$^4P_{5/2}$	1	60.953	60.597	0.054	0.020	0.024	0.056
	$^4P_{3/2}$	2	60.891	60.552	0.015	0.006	0.003	0.012
	$^4D_{7/2}$	3	60.723	60.367	0.010	0.006	0.006	0.009
	$^4P_{1/2}$	3	60.688	60.367	0.001	0.002	0.019	0.003
	$^2D_{5/2}$	4	60.665	60.331	0.033	0.012	0.005	0.034
	$^2D_{3/2}$	5	60.341	60.045	0.099	0.034	0.062	0.138
	$^2P_{1/2}$	6	60.229	59.955	0.027	0.011	0.010	0.038
	$^9D_{5/2}$	9	60.177	59.830	0.006	0.002	0.001	0.006
	$^2P_{1/2}$	7	60.170	59.824	0.013	0.005	0.003	0.013
	$^2P_{3/2}$	8	60.120	59.827	0.028	0.011	0.009	0.025
	$^4S_{3/2}$	11	59.962	59.597	0.013	0.005	0.010	0.015
	$^4D_{3/2}$	12	59.858	59.631	0.026	0.008	0.024	0.025
	$^4D_{1/2}$	10	59.807	59.551	0.012	0.005	0.012	0.014
$4p^4(^1D)5p$	$^2F_{5/2}$	13	58.700	58.706	0.016	0.008	0.009	0.016
	$^2F_{7/2}$	14	58.641	58.641	0.128	0.136	0.106	0.109
	$^2P_{3/2}$	15	58.427	58.579	0.242	0.118	0.075	0.194
	$^2D_{5/2}$	16	58.305	58.317	0.097	0.050	0.054	0.096
	$^2D_{3/2}$	18	58.280	58.332	0.010	0.005	0.058	0.068
	$^2P_{1/2}$	17	58.137	58.326	0.072	0.040	0.001	0.072
$4p^4(^1S)5p$	$^2P_{1/2}$	19	56.689	56.339	0.000	0.000	0.000	0.000
	$^2P_{3/2}$	20	56.678	56.256	0.234	0.117	0.145	0.229

TABLE III. Calculated intensities (in 10^{-3} a.u.) for the Kr $3d_{3/2}^{-1}5p \rightarrow 4p^{-2}5p$ resonant Auger transitions. FE is the same as in Table II. FEI is the same as FE, but IISCI was calculated using initial-state orbitals. FEO is the same as FE, but IISCI was omitted.

Final ionic state		Initial state *B*				Initial state *C*			
Parent	Term	FE	FEI	FEO	Chen [19]	FE	FEI	FEO	Chen [19]
$4p^4(^3P)5p$	$^4P_{5/2}$	0.018	0.017	0.014	0.054	0.002	0.003	0.007	0.007
	$^4P_{3/2}$	0.005	0.009	0.001	0.028	0.006	0.001	0.009	0.005
	$^4D_{7/2}$	0.008	0.004	0.012	0.011	0.003	0.007	0.000	0.019
	$^4P_{1/2}$	0.000	0.000	0.000	0.000	0.000	0.000	0.000	0.000
	$^2D_{5/2}$	0.003	0.004	0.008	0.005	0.017	0.016	0.012	0.052
	$^2D_{3/2}$	0.002	0.007	0.007	0.004	0.026	0.021	0.021	0.044
	$^2P_{1/2}$	0.003	0.003	0.002	0.003	0.000	0.000	0.003	0.000
	$^4D_{5/2}$	0.033	0.016	0.043	0.046	0.010	0.026	0.001	0.073
	$^2P_{1/2}$	0.001	0.002	0.000	0.009	0.005	0.003	0.005	0.009
	$^2P_{3/2}$	0.010	0.015	0.003	0.013	0.008	0.004	0.015	0.034
	$^4S_{3/2}$	0.007	0.002	0.015	0.077	0.010	0.015	0.002	0.019
	$^4D_{3/2}$	0.030	0.032	0.016	0.049	0.005	0.002	0.019	0.025
	$^4D_{1/2}$	0.004	0.001	0.006	0.000	0.002	0.005	0.000	0.010
$4p^4(^1D)5p$	$^2F_{5/2}$	0.054	0.112	0.019	0.109	0.139	0.080	0.173	0.145
	$^2F_{7/2}$	0.095	0.047	0.128	0.050	0.032	0.081	0.000	0.085
	$^2P_{3/2}$	0.030	0.020	0.044	0.113	0.024	0.035	0.031	0.087
	$^2D_{5/2}$	0.094	0.063	0.109	0.136	0.047	0.077	0.030	0.102
	$^2D_{3/2}$	0.048	0.104	0.006	0.150	0.112	0.055	0.154	0.009
	$^2P_{1/2}$	0.038	0.020	0.045	0.065	0.009	0.026	0.000	0.050
$4p^4(^1S)5p$	$^2P_{1/2}$	0.041	0.109	0.000	0.220	0.140	0.072	0.180	0.156
	$^2P_{3/2}$	0.120	0.053	0.173	0.108	0.055	0.121	0.001	0.249

The calculated values for the initial states *B* and *C* are given in Table III. The IISCI is of great importance in the case of these transitions, which can be seen when comparing the FE, FEI, and FEO results to one another. The three results differ only in that respect that they involve different initial-state mixing coefficients, but the changes in the intensity distribution are dramatic.

IV. COMPARISON BETWEEN EXPERIMENT AND THEORY

A. Transition energies

A comparison between the experimental and calculated absolute energies given in Table II for the $3d_{5/2}^{-1}5p \rightarrow 4p^{-2}5p$ transitions shows a difference of 0.1–0.3 eV. The relative energies are not very well reproduced by the average level SCF calculations for the final state, which include the FISCI as decribed above. Even the order of some levels differs in theory as compared with experiment.

The energy splitting was, furthermore, found to be very sensitive to the orbital set. When predicted by initial-state orbitals, the splitting decreased substantially and also the order of levels changed. The optimization method, and especially the basis set used in calculations, is thus of crucial importance in reproducing the energy level structures. Their choice affects not only the eigenvalues but also the eigenvectors. The disagreement in energy splitting may thus indicate some failure in the determination of intensity distribution as well.

B. Partial transition rates

1. The $3d_{5/2}^{-1}5p_{3/2}$ resonant Auger spectrum

A comparison between experiment and theory shows that the distribution of the intensity to the fine-structure components produced by the spectator-core coupling from the parent multiplets is fairly well reproduced by all the calculations in the case of the $3d_{5/2}^{-1}5p \rightarrow 4p^{-2}5p$ transitions. The differences are the most distinct for the transitions to the $4p^4(^3P)5p(^2D_{3/2})$ (line 5) and the $4p^4(^1D)5p(^2F_{7/2})$ (line 14) final states. In the case of line 5, the calculations tend to underestimate the relative intensity of transitions. The intensity of line 14 is, on the other hand, very sensitive to the calculation method. The *F* approximation seems to reproduce the intensity of line 14 fairly well, whereas the FE approximation overestimates the intensity by about a factor of 2. This transition is dominated by the $\epsilon\, g_{9/2}$ transition amplitude, which is very sensitive to the exchange interaction.

Except for line 14, the relative line intensities do not essentially vary when passing from the *F* to the FE approximation. The differences between the FE and IE results are more distinct. The FE approach seems to reproduce the experiment slightly better than IE in most cases if line 14 is excluded. Only the transitions to the final states with total angular momentum value $J=3/2$ are not quite properly predicted by the FE calculations. The intensity of line 15 is clearly overestimated, whereas the intensity of line 18 is underestimated, by the FE approach. The IE calculations, however, give just the opposite results, which indicates that the eigenvectors, especially for the $J=3/2$ states, vary consider-

ably when obtained with the initial- or final-state orbital set. For the final-states $J=1/2$ and $J=5/2$ the FE approach is clearly preferable as compared to the IE approach. This indicates that the mixing coefficients, obtained from a calculation with final-state orbitals, are fairly well suited to the prediction of partial transition rates.

2. The $3d_{3/2}^{-1}5p_{1/2,3/2}$ resonant Auger spectrum

The $3d_{3/2}^{-1}5p$ spectrum is entirely determined by the transitions from the initial state B of Table III, if the assumption that the photoexcitation branching ratio is properly reproduced by theory holds. By comparing the relative intensities calculated in different approximations for both states B and C (Table III) with experiment, the FEI results for state B seem to give the best resemblance. On the other hand, the calculated intensity distributions for the initial state C seem to differ considerably from the experiment. This confirms the prediction that state C is not remarkably populated via photoexcitation. The FEI calculation for the initial state B seems to predict a reversed intensity ratio for the transition to the final states, with $J=3/2$, that corresponds to lines 15 and 18. This can be traced back to the inconsistency in the eigenvectors of the final states, which was seen to alter the relative intensities of the same lines in the case of transitions from the $3d_{5/2}^{-1}5p$ initial state (state A) as well.

The three results FE, FEI, and FEO, all differ distinctly from one another, and only the FEI approach is capable of reproducing the experiment. This indicates that eigenvectors of the initial states and the basis set used in their calculation are of special importance. The sensitivity of the $3d_{3/2}^{-1}5p$ resonant Auger transitions to the mixing of configurations both in the initial and final states of the decay makes it very difficult to find an excellent agreement with experiment. This sensitivity, however, offers a useful method to test the strength of interaction between the core and the spectator electron, since it displays the changes in the intermediate-coupling conditions easily.

C. Comparison between Kr and Xe results

The close analogy between the resonant Auger spectra of Kr studied in this work and of Xe reported recently [2,3] makes it possible to make an interesting comparison between them. The transitions in Kr and Xe involve analogous orbitals; the principal quantum number only increases by 1 in the case of Xe. This has, however, such an effect that kinetic energies of emitted electrons are by about a factor of 2 larger in Kr as compared to Xe. Higher kinetic energies clearly reduce the importance of exchange interaction, which is seen in the fact that deviations between the F and FE results are larger in Xe than in Kr. The transitions to the $J=7/2$ final state, strongly affected by the exchange effect, are not properly reproduced by theory in both Xe and Kr, but the discrepancy is not as pronounced in Kr as in Xe. Surprisingly, the $4d_{5/2}^{-1}6p\rightarrow 5p^4(^1D)6p(^2F_{7/2})$ transitions are very weak in Xe, whereas the $3d_{5/2}^{-1}5p\rightarrow 4p^4(^1D)5p(^2F_{7/2})$ transitions of Kr result in a strong peak in the experiment, even though about the same relative ratios are predicted by theory in both cases. In an earlier study of the normal Auger transitions [17], the channel mixing was observed to partly revise the influence of exchange interaction. The mixing of continuum channels was found to be more important in Xe than in Kr because of the lower kinetic energies of Xe Auger electrons. Whether the resonance Auger transitions behave in a similar way needs to be studied separately.

The IISCI and FISCI were found to affect the partial transition rates in a very similar way in both Xe and Kr. Thus the spectator electron on the first empty orbital results in a strong core-spectator interaction, and the relative strength of that interaction as compared to the core-core interaction is hardly predicted by theory. Extended multiconfiguration calculations are needed to arrive at a better description of the mixing of configurations in intermediate coupling.

V. CONCLUSIONS

The elimination of the lifetime broadening in the resonant Auger spectra has been possible by utilizing the Auger resonant Raman effect both in Xe [2,3] and in Kr (this work). Comparison between experiment and theory has made it possible to confirm the roles of exchange interaction and of IISCI and FISCI in distributing the intensity to the fine structures in the spectra.

The exchange interaction was found to be of importance when the transitions are dominated by amplitudes where continuum electrons have large orbital angular momentum values. Its role diminishes quickly, however, with increasing kinetic energy of Auger electrons. Intermediate-coupling conditions are easily affected by the interaction between the core and the spectator electrons. The FEI approximation, accounting for the exchange interaction as well as the IISCI and FISCI effects, was found to agree fairly well with the experiment, although hints from the existence of additional correlation effects were also seen.

ACKNOWLEDGMENTS

The authors would like to thank Dr. S. Svensson and his group for the opportunity to use their electron spectrometer. The staff of MAX-laboratory is acknowleged for assistance during the measurements. This work has been supported by the Research Council for the Natural Sciences of the Academy of Finland.

[1] A. Kivimäki, A. Naves de Brito, S. Aksela, H. Aksela, O.-P. Sairanen, A. Ausmees, S. J. Osborne, L.B. Dantas, and S. Svensson, Phys. Rev. Lett. **71**, 4307 (1993).

[2] H. Aksela, S. Aksela, O.-P. Sairanen, A. Kivimäki, A. Naves de Brito, E. Nõmmiste, J. Tulkki, S. Svensson, A. Ausmees, and S.J. Osborne, Phys. Rev. A **49**, R4269 (1994).

[3] H. Aksela, O.-P. Sairanen, S. Aksela, A. Kivimäki, A. Naves de Brito, E. Nõmmiste, J. Tulkki, A. Ausmees, S.J. Osborne, and S. Svensson, Phys. Rev. A **51**, 1291 (1995).

[4] O.-P. Sairanen, H. Aksela, S. Aksela, J. Mursu, A. Kivimäki, A.

Naves de Brito, E. Nõmmiste, S.J. Osborne, A. Ausmees, and S. Svensson, J. Phys. B **28**, 4509 (1995).
[5] S. Aksela, A. Kivimäki, A. Naves de Brito, O.-P. Sairanen, S. Svensson, and J. Väyrynen, Rev. Sci. Instrum. **65**, 831 (1994).
[6] S. Aksela, A. Kivimäki, O.-P. Sairanen, A. Naves de Brito, and S. Svensson, Rev. Sci. Instrum. **66**, 1621 (1995).
[7] J. Tulkki, H. Aksela, and N.M. Kabachnik, Phys. Rev. A **50**, 2366 (1994).
[8] H. Ahola and T. Meinander, Rev. Sci. Instrum. **63**, 372 (1992).
[9] Å. Andersson, S. Werin, T. Meinander, A. Naves de Brito, and S. Aksela, Nucl. Instrum. Methods Phys. Res. Sect. A **362**, 586 (1995).
[10] R. Nyholm, S. Svensson, J. Nordgren, and A. Flodström, Nucl. Instrum. Methods **246**, 267 (1986); S. Aksela, A. Kivimäki, R. Nyholm, and S. Svensson, Rev. Sci. Instrum. A **63**, 1252 (1992).
[11] S.J. Osborne, A. Ausmees, J.O. Forsell, B. Wannberg, G. Bray, L.B. Dantas, S. Svensson, A. Naves de Brito, A. Kivimäki, and S. Aksela, Synchrotron Radiat. News **7**(1), 25 (1994). The spectrometer has been provided by the research group of Dr. S. Svensson, Department of Physics, University of Uppsala.
[12] G.C. King, M. Tronc, F.H. Read, and R.C. Bradford, J. Phys. B **10**, 2479 (1977).
[13] H. Aksela, G.M. Bancroft, and B. Olsson, Phys. Rev. A **46**, 1345 (1992).
[14] C.E. Moore, *Atomic Energy Levels*, edited by L.M. Branscomb, Natl. Bur. Stand. (U.S.), Circ. No. 467 (U.S. GPO, Washington, DC, 1952), Vol. II.
[15] J. Jauhiainen, A. Ausmees, A. Kivimäki, S.J. Osborne, A. Naves de Brito, S. Aksela, S. Svensson, and H. Aksela, J. Electron Spectrosc. Relat. Phenom. **69**, 181 (1994).
[16] J. Tulkki, T. Åberg, A. Mäntykenttä, and H. Aksela, Phys. Rev. A **46**, 1357 (1992).
[17] J. Tulkki, N. Kabachnik, and H. Aksela, Phys. Rev. A **48**, 1277 (1993).
[18] K.G. Dyall, I.P. Grant, C.T. Johnson, F.A. Parpia, and E.P. Plummer, Comput. Phys. Commun. **55**, 425 (1989).
[19] M.H. Chen, Phys. Rev. A **47**, 3733 (1993).